Effect of splitter blades on turbine mode of low specific speed pump

Jiří Bezdíček[1*], *Lilian* Chabannes[1], and *David* Štefan[1]

[1]V. Kaplan Department of Fluid Engineering, Faculty of Mechanical Engineering, Brno University of Technology, Technická 2896/2, 61699 Brno, Czech Republic

Abstract. The use of pump in turbine mode is an evolving research field. This article is mainly focused on the influence of splitter blades on the turbine mode of pump exclusively. CFD analysis on low specific speed pump geometry was performed. The geometry of sidewall gaps spaces between the rotor and stator system was also included in the computational model. Flow phenomena were compared with quantification of losses. In this case, entropy production theory was used for loss analysis. The effect of different computational meshes and turbulence models on the low-specific speed machine was also questioned. The numerical approach was used not only to obtain turbine characteristics and evaluate the effect of splitter-blades on the machine, which was main goal of this work but also to describe flow or carry out hydraulic loss analysis and visualise areas of most dominant losses. Volumetric efficiency, hydraulic forces, and influence of flow in sidewall gaps on torque generation were also investigated. The numerical model was validated using experimental data. Probable reasons for the difference between the experiment and simulation were estimated.

1 Introduction

One of the most convenient ways to generally classify types of hydrodynamic pumps is by a similarity criterion called specific speed.

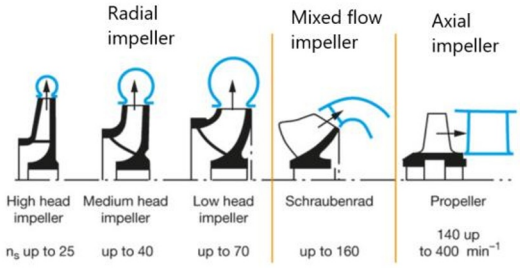

Fig. 1. Classification of impeller types based on specific speed according to KSB [1].

$$n_s = 3{,}65 \cdot n \cdot \frac{Q^{0.5}}{H^{0.75}} \qquad (1)$$

The specific speed is defined by equation (1), where n_s [min^{-1}] is the specific speed, n [min^{-1}] is the impeller speed, Q [m^3·s^{-1}] is the flow rate and H [m] is the head.

Low-specific speed pumps are, from the geometrical point of view, specific with their exclusively radial output of flow, thus large diameter of the impeller and narrow meridional section [2]. Advantages but also many disadvantages are bounded with these geometric constrains. Among the most well-known disadvantages are low efficiency, instability of head characteristics at low flow rates and most importantly significant disk losses which are given by the large diameter of the impeller [3]. However, this type of machine can be useful despite all its disadvantages. It can be used, for example, where it is necessary to overcome large heads where it can provide a better economic solution as opposed to multistage pumps or even to more pumps connected in series.

Pumps running in the turbine mode (PaTs) are becoming more common due to their cost-effectiveness in comparison with conventional turbines. The main economic advantage consists in initial investment. Even though use of the standard radial centrifugal pumps from the middle of the specific speed spectrum has already been investigated by many researchers [4, 5, 6], low-specific speed pumps have not yet been extensively investigated in the turbine mode. Only a few researchers have dealt with this specific type of PaT [7, 8]. Although conclusions from these studies can be used to compare results of this work, these PaTs fall only to the upper limit of low specific speed range.

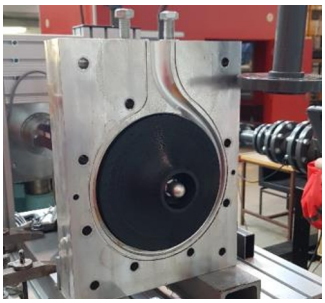

Fig. 2. Assembly of low specific speed pipe, author Lilian Chabannes.

* Corresponding author: Jiri.Bezdicek@vut.cz

As mentioned, this article focuses on the turbine mode of a very low specific speed pump of $n_s = 32$ developed during PhD project by Lilian Chabannes [9].

Use of Low Specific speed (LSS) machine specifically in turbine mode could have many applications. For example, it can be a cost-effective alternative to a crossflow turbine. Theoretically, Pelton turbine or low specific speed Francis' turbine can be also replaced by LSS PaT. The range of applicability of the single-stage pumps in turbine mode in terms of head H [m] and flow rate Q [m^3/s] is shown in Figure 3.

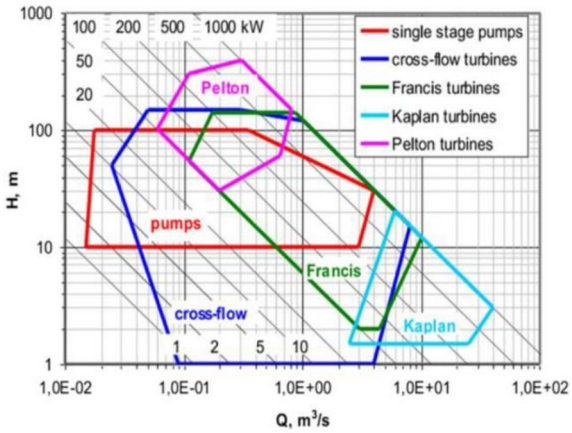

Fig. 3. Working spectrum of PaTs (red color) in comparison with conventional turbines [10].

Advantages of (LSS) PaT can be also utilized in water distribution networks (WDNs), where Pressure reduction valves (PRV) are replaced by PaTs for not only pressure reduction, but also for an energy recuperation purpose. However, in this field of use, there are many obstacles which must be overcome. The main obstacle is the considerable hydraulic efficiency characteristic drop in non-optional working conditions of PaT in comparison with conventional turbines, where drop is not so significant due to the possibility of controlling the angle of attack on the leading edge of blades [10, 11]. As there are always changing pressure and flow conditions in WDNs, which is given by variable water demand (the main difference occurs between day and night) [12]. Power drop in non-optional conditions is fundamental problem and hydraulic or electric regulation is often needed [13].

Another aspect is the safe operation of PaT in such network, where in case of machine shut off the flow must be remained without significant pressure increase. Thus, some safety measures must be included, e. g. in a form of the bypass.

This article provides extended results of the first author's diploma thesis [14].

2 Pump specifications

Geometry of LSS PaT was adopted from [9]. Volute was CNC machined and impellers were 3D printed and the rest of casing was adopted from common industrial pump. Geometry specifications and other design parameters of investigated pump can be seen in Table 1, where H_d stands for design head,Q_d is design flow rate, z is number of blades, D_2 is the outer diameter of the impeller, b_2 is outlet width of impeller and $\beta_{2L}$is outlet angle of blade.

Table 1. Design parameters of investigated PaT.

Parameters	Values	Units
n_s	32	[min^{-1}]
n	1450	[min^{-1}]
H_d	12,5	[m]
Q_d	0,00168	[m^3 s^{-1}]
z	4	[-]
D_2	200	[mm]
b_2	3,75	[mm]
β_{2L}	25	[º]

Main goal of this work was to assess the splitter blades effect on turbine mode performance. Three layouts from Fig 4 were compared to each other.

Fig. 4. Impeller layouts, From the left side: 0splitter, 1splitter and 2splitter.

The first layout (0splitter) consisted of four main blades. The second layout (1splitter) contained the main blades but also four splitter blades were added. Finally, third layout (2splitter) consisted of four main blades and two sets of splitter blades. These configurations were created for optimal pump mode operation [9]. Goal of this work was to assess if splitter blades exclusively designed for pump mode will have positive effect in turbine mode as in pump mode without any further modifications.

3 Entropy production theory

One of the methods for analysing losses is the entropy production theory [15, 16]. This approach is easy to apply and has the significant advantage of being able to visualise areas of the losses. Assuming transport equation for specific entropy [15]:

$$\rho \cdot \left(\frac{\partial s}{\partial t} + u\frac{\partial s}{\partial x} + v\frac{\partial s}{\partial y} + w\frac{\partial s}{\partial z}\right) = -div\left(\frac{\bar{q}}{T}\right) + \frac{\Phi}{T} + \frac{\Phi_\theta}{T^2} \quad (2)$$

Where s [J · kg^{-1} · K^{-1}] is specific entropy, u,v and w [m/s] are velocity vector components according to cartesian coordinate system, $\bar{q}$ is heat flux vector, T [K] is temperature and ρ [kg · m^{-3}] is density. Last term in the equation stands for entropy generation by heat transfer. Second term from the right-hand side is entropy generation caused by dissipation. Both these terms can be divided into time-averaged component and fluctuation component [15,16].

For a considerable number of simulations, a constant temperature is considered, i.e., an isothermal process is applied to numerical model. In this case we can neglect entropy production generated by the heat transfer and then, only source term left is associated with dissipation in the investigated system.

$$\frac{\Phi}{T} = \overline{S_D} + \acute{S_D} \tag{3}$$

If we divide dissipation source term in two components, then averaged component $\overline{S_D}$ stands for direct dissipations and fluctuation component $\acute{S_D}$ stands for turbulent dissipation [15].

$$\overline{S_D} = \frac{\mu}{T} \cdot \left\{ 2\left[\left(\frac{\partial \bar{u}}{\partial x}\right)^2 + \left(\frac{\partial \bar{v}}{\partial y}\right)^2 + \left(\frac{\partial \bar{w}}{\partial z}\right)^2 \right] + \left(\frac{\partial \bar{u}}{\partial y} + \frac{\partial \bar{v}}{\partial x}\right)^2 + \left(\frac{\partial \bar{u}}{\partial z} + \frac{\partial \bar{w}}{\partial x}\right)^2 + \left(\frac{\partial \bar{v}}{\partial z} + \frac{\partial \bar{w}}{\partial y}\right)^2 \right\} \tag{4}$$

The μ quantity in the equation (4) is the viscosity, some literature define it as effective viscosity, which is the sum of the molecular and turbulent viscosities [16]. Other literature does not specify which viscosity is consider [15]. $\bar{u}, \bar{v}, \bar{w}$ are components of time-averaged velocity vector. The source term $\overline{S_D}$ that is related to direct dissipation can be easily determined from the results of a CFD simulation [15]. Velocity components from the steady state simulation can be used. Transient simulation results can also be used to obtain more accurate results, but the time-averaged values are preferred to be used. In this article results from transient simulations were processed.

The fluctuating source term $\acute{S_D}$ can be approximately calculated using the turbulence dissipation rate ε, density ρ and constant temperature T according to the following relation. As this term is not directly obtainable by CFD calculation [15].

$$\acute{S_D} = \frac{\rho \cdot \varepsilon}{T} \tag{5}$$

Dissipation near the wall can be estimated by following equation [15]

$$S_w = \frac{\tau_w \cdot \bar{w}}{T} \tag{6}$$

S_w is associated with entropy production near the wall, τ_w is wall shear stress and $\bar{w}$ is average velocity in the middle of first layer of finite volumes near the wall [15].

4 Experimental setup

Experiment was carried out at laboratory of Victor Kaplan Department of Fluid Engineering.

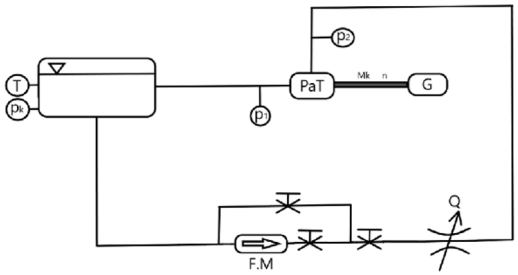

Fig. 5. Test rig of PaT.

Flow rate, temperature and pressure in discharge tank and pressures in front and behind PaT were measured. Efforts were made to maintain a constant head using a feed pump, frequency converter and a set of valves. A head value of 21 m was chosen as expected value of maximal efficiency for pump's nominal speed.

For comparability of CFD results with measured data, correction of torque regarding mechanical losses was carried out. With impeller removed, shaft itself was rotated in the water and static torque was measured for different rotation speeds. The correction torque, which should correspond to the CFD calculated torque, was subsequently given by the sum of the measured torque and the static torque. It must be noted that torque correction is without effect of hydraulic forces which would act on the impeller.

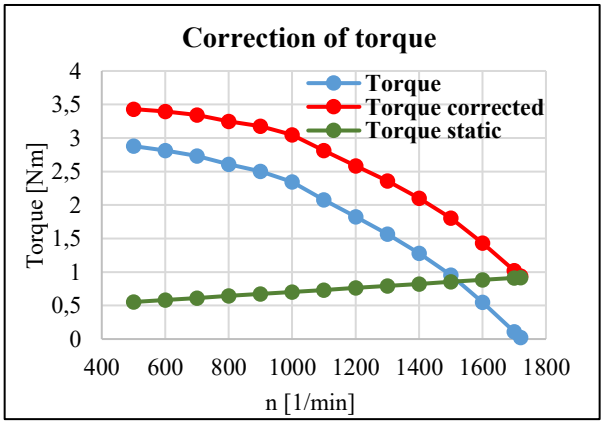

Fig. 6. Torque correction.

5 Numerical model

Numerical analysis was carried out in commercial code Ansys CFX R21. Discretization of the impellers was performed in the TurboGrid pre-processor. The mesh of outlet pipe was done in ICEM CFD, and mesh of the volute was created in Ansys meshing as well as the sidewall gaps. The overall fluid domain consisted of five individual domains that were connected using appropriate interfaces. The individual domains, including the number of nodes, are summarized in the following table.

Table 2. Computational mesh size.

Domain	Number of nodes [-]
0splitter Impeller	$1{,}057 \cdot 10^6$
1splitter Impeller	$1{,}426 \cdot 10^6$
2splitter Impeller	$1{,}717 \cdot 10^6$
Volute (Including inlet pipe)	$0{,}699 \cdot 10^6$
Outlet pipe	$1{,}494 \cdot 10^6$
Sidewall gap at shroud disc side (SGS)	$1{,}791 \cdot 10^6$
Sidewall gap at shroud disc side (SGH)	$0{,}325 \cdot 10^6$

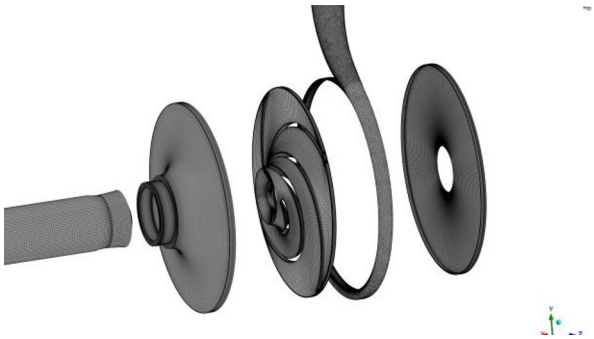

Fig. 7. Five computational domains in displacement for presentation purposes, from left: Outlet pipe, Sidewall gap at shroud disc side (SGS), Impeller, Volute, Sidewall gap at hub disc side (SGH).

In each of the pre-processors used, qualitative parameters were monitored. In the ICEM CFD, in which the outlet pipe mesh was created, these were the "angle parameter", which reached a minimum value of 27.08, and the "aspect ratio", which reached a maximum value of 14.4. In Ansys meshing (volute domain) the "skewness" and “aspect ratio” was monitored. The maximum value of skewness was 0.88 and the aspect ratio globally reached values below 80. Finally, for the sidewall gaps maximum skewness was 0.00418 and maximum aspect ratio was 8.29. The quality parameters in TurboGrid monitored automatically. Worst mesh quality globally was detected in domain of volute.

In addition, a study of independence from the computational mesh was performed. Three computational meshes were compared for the 1splitter variant in BEP. The monitored variables were flow rate and hydraulic efficiency.

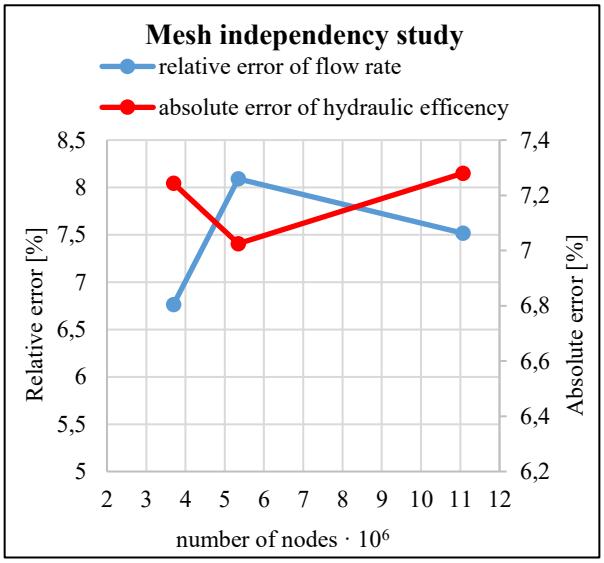

Fig. 8. Mesh independency study.

The results show that in terms of flow rate, the smallest error was achieved for the mesh with the smallest number of nodes. However, for this mesh it was assumed that it would not be suitable for non-optimal operating conditions, which are also addressed in this paper. For this reason, a medium sized mesh was chosen for computation of all investigated operating conditions. Although this mesh had the largest error in the flow rate, the efficiency was closest to the experiment. The largest mesh, which showed a smaller error in flow rate but also had an increased error in efficiency, was not used to ensure reasonable simulation time.

The impeller was set as a rotating domain for each case, the remaining domains were always considered stationary. For walls in the stationary domain belonging to the impeller, an angular velocity was prescribed.

For each transient calculation performed, initial data were first obtained by stationary calculation. In this case, the rotational domains were connected using the "Frozen rotor" interface. For subsequent transient calculations, the "Transient Rotor Stator" interface was used. The stationary domains were connected in all cases using the GGI interface.

The implicit type of boundary conditions was set to match the constant head of 21 m, as in the experiment. This was done by prescribing a total pressure at the inlet and a static pressure at the outlet.

The standard k- ε turbulence model with scalable wall function was used.

For comparability purposes, the characteristics were plotted in n_{11}, Q_{11} and η_h quantities, which are the usual standard for turbine characteristics.

6 Splitter blades effect

The main goal of work was to assess influence of splitter blades on performance of low specific speed PaT. Change in the hydraulic efficiency η_h between the three impeller variants were monitored for the selected operating points.

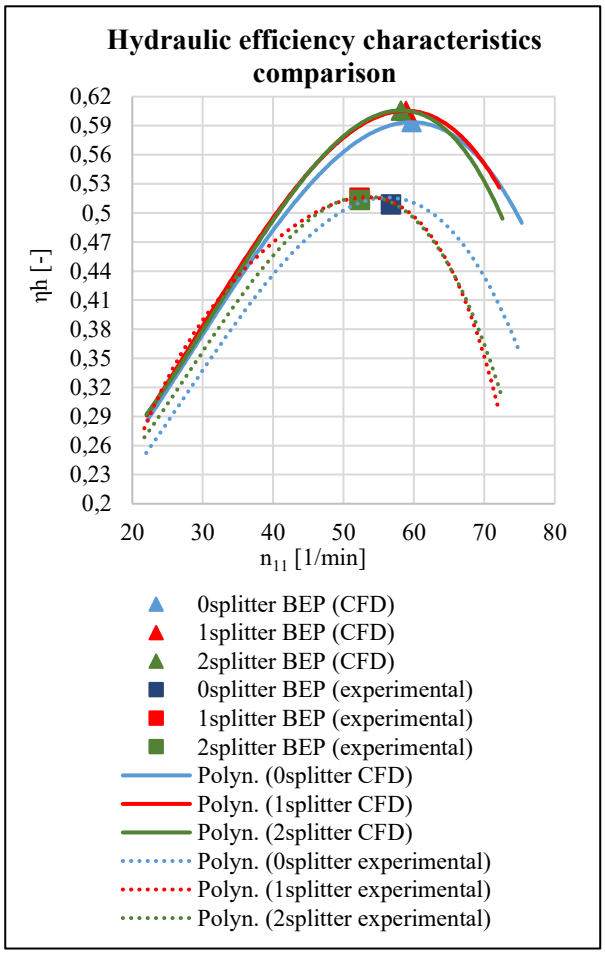

Fig. 9. Hydraulic efficiency, CFD and experiment.

The hydraulic efficiency predicted by the numerical model was overestimated in comparison with experiment. Even so, it was possible to evaluate the effect of the addition of the splitter blades from the characteristics obtained.

The main effect of adding the splitter blades was a shift of the optimum (BEP) to lower unit speeds for both splitter blade variants of impeller. This phenomenon occurred for both CFDs and experiment.

It was evident from the experiment and CFD that at the optimum both splitter variants also had a slight increase in the efficiency. However, the increase was relatively small. The largest increase with respect to the impeller without splitter blades was achieved for the 1splitter variant in the order of tenths of a percent.

The main reason for the over-prediction of hydraulic efficiency was probably the different roughness of the physical model, which was made by 3D print technology, and the ideal geometry with smooth walls from CFD. The roughness and specific patterns of the impeller walls in combination with high disc friction losses probably caused the described error.

Relative characteristics were plotted to determine the accuracy and suitability of the numerical model used. For the relative characteristics, the unit flow and unit hydraulic efficiency were always related to the value of BEP.

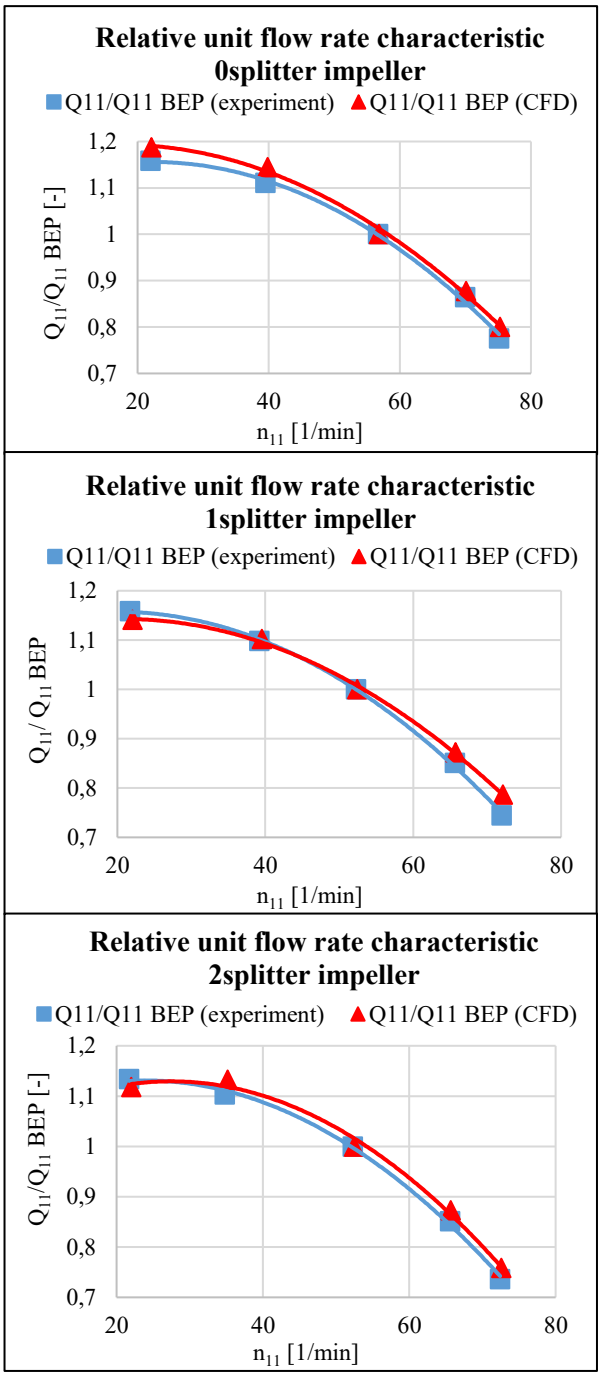

Fig. 10. Relative characteristics of flow rate for each impeller variant.

Relative characteristics of unit flow rate obtained by CFD were in agreement with experimental data only with small deviations. The most notable deviation was spotted for 0splitter variant in lowest n_{11} operating condition. One of the discrepancy reasons might be the turbulence model which is not suitable for such off-design regime with secondary flow. Another aspect might be the discrepancy due to particular deformation of physical 3D printed impeller.

Hydraulic efficiency was overestimated in over-load operating conditions. The numerical model therefore did not correctly predict the measured nature of the flow.

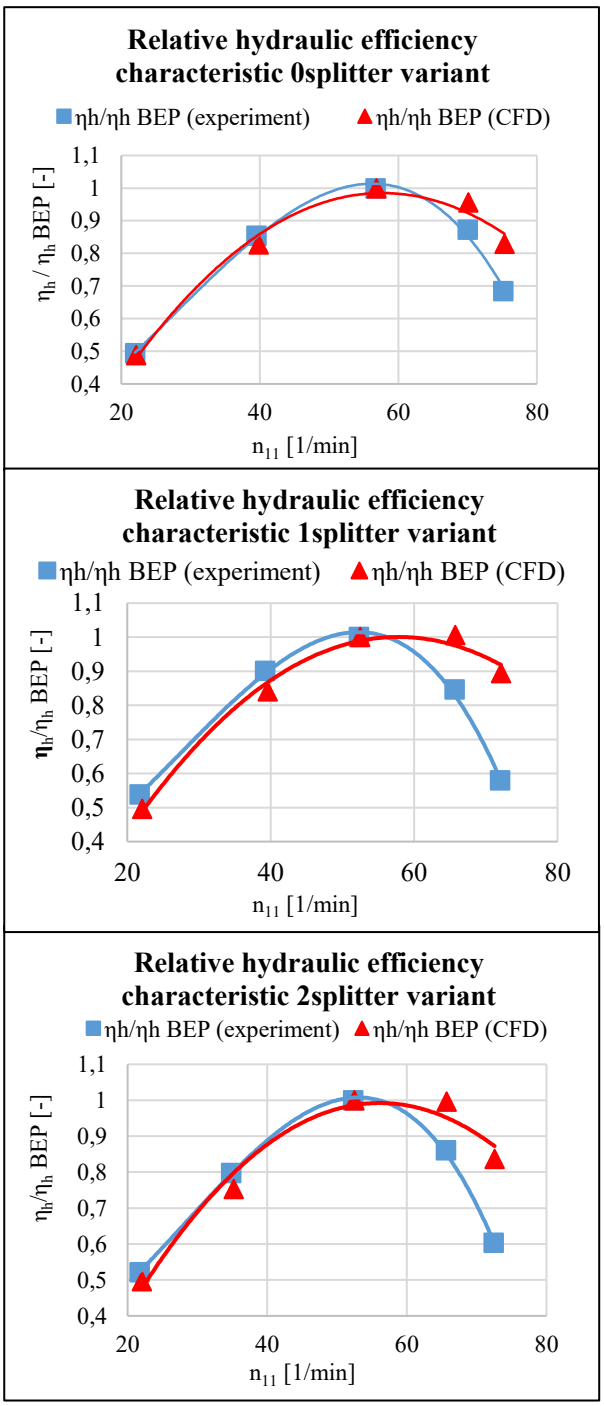

Fig. 11. Relative characteristics of hydraulic efficency for each impeller variant.

Error in over-load operating conditions was probably given by low-Re turbulence model employing the scalable wall function. Wall functions probably incorrectly determined the losses in the areas with higher dissipation. This phenomenon was previously described by Juckelandt [17], Chabannes [18] and also by Wang, studying applicability of eddy viscosity turbulence models [19].

7 Loss analysis

Due to the specific geometry of investigated PaT, many unsteadinesses were found in simulated flow field. There was a swirling character of the flow in the outlet pipe, which is a standard problem of pumps running in turbine mode [7]. Among non-stationarities which developed directly in the impeller, there was the local eddy on suction or pressure side of blades, depending on the operating conditions. At part-load operating conditions, there was also a so-called pumping effect, where the flow was separated in the impeller and part of the liquid always returned to the spiral. Pumping effect was attenuated at BEP operating condition and at higher unit speeds.

The local vortex was at its largest size at the lowest unit speed. For this reason, the different impeller variants were compared with each other for this respective n_{11}. All contours were time-averaged by four revolutions of the impeller.

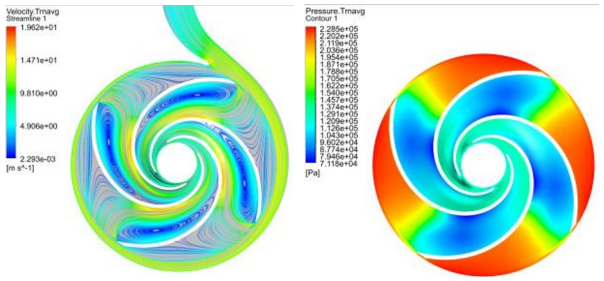

Fig. 12. Surface streamlines and static pressure at lowest n_{11}, 0splitter

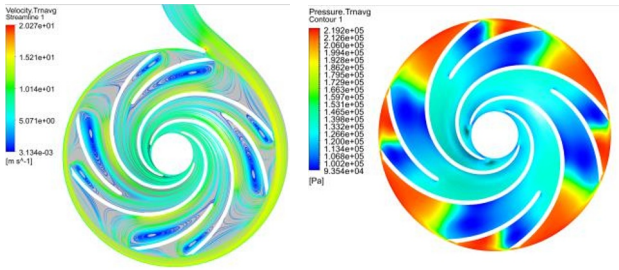

Fig. 13. Surface streamlines and static pressure at lowest n11, 1splitter

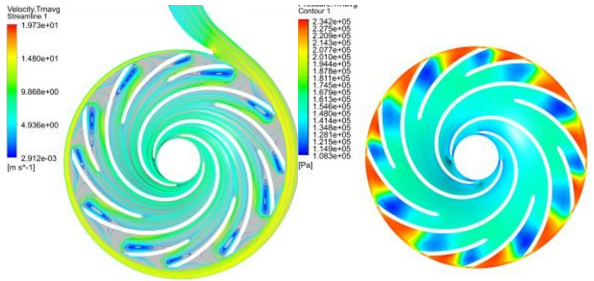

Fig. 14. Surface streamlines and static pressure at lowest n11, 2splitter.

Figures 12, 13 and 14 show that the addition of splitter blades dampens the eddies on the suction side of the blade. However, eddies also form on the added splitter blades, which is probably the reason why adding splitter blades has not resulted in a substantial increase in PaT performance.

To investigate the eddy behaviour depending on the operating condition, surface streamlines were plotted in the split plane of the impeller for the 0splitter and 2splitter variants. The operating conditions of lowest n_{11} and highest n_{11} and the optimum (BEP) were selected. From depicted surface streamlines it was possible to analyse effect of splitter blades for three chosen operating conditions.

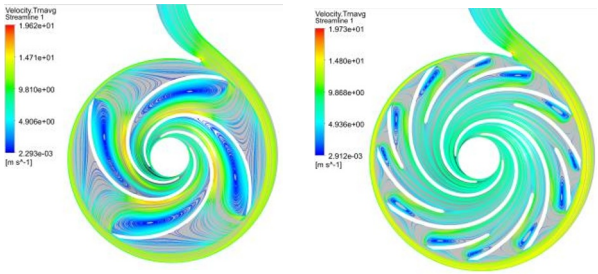

Fig. 15. 2D streamlines, lowest n_{11}, 0splitter and 2splitter variant

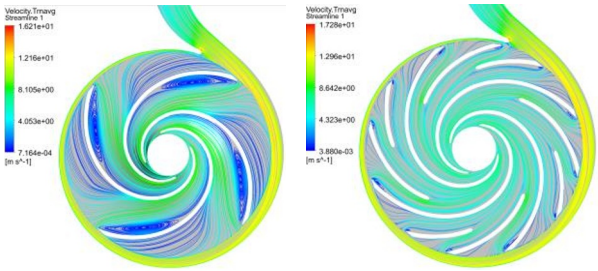

Fig. 16. 2D streamlines, BEP, 0splitter and 2splitter variant.

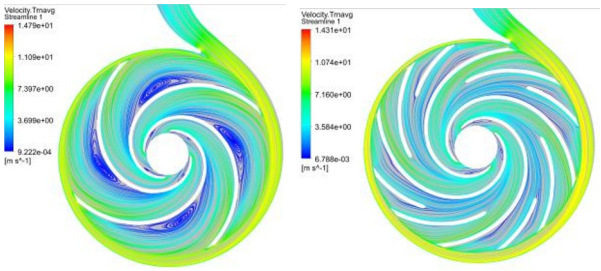

Fig. 17. 2D streamlines, highest n_{11}, 0splitter and 2splitter variant.

When the PaT was operated in BEP and at the lowest n_{11}, the local eddy was located on the suction side of the blades. The main cause of this vortex was probably the sharp leading edge of the blade, which made the eddy formation sensitive to the angle of incidence, i.e., angle of flow. At the highest n_{11}, the vortex formed on the pressure side of the blade. This was probably due to the negative incidence of the inflow. Splitter blades in this case successfully helped to attenuate eddy on pressure side of blade.

The vortex had its largest dimensions at the lowest n_{11}. Particularly in this operating condition the separation of the flow inside the impeller occurred, and part of the fluid returned to the volute, a phenomenon that could be described as the pumping effect.

The swirling nature of the flow in the outlet pipe is presented in all operating conditions investigated for all impeller variants. For simple qualitative analysis 3D streamlines were plotted. Lowest n_{11}, BEP and highest n_{11} of 1splitter variant were chosen.

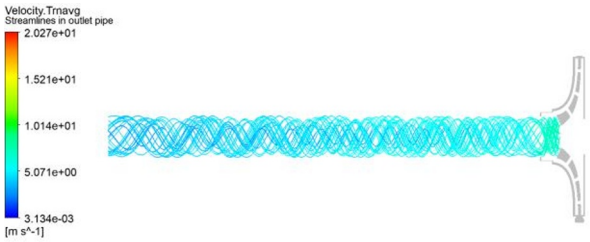

Fig. 18. 3D streamlines in outlet pipe, 1splitter impeller, n_{11} = 22,04 min^{-1}

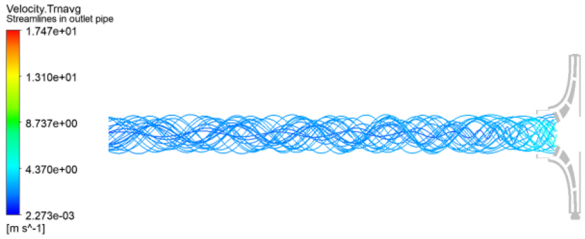

Fig. 19. 3D streamlines in outlet pipe, 1 splitter impeller, n_{11} = 52,45 min^{-1}

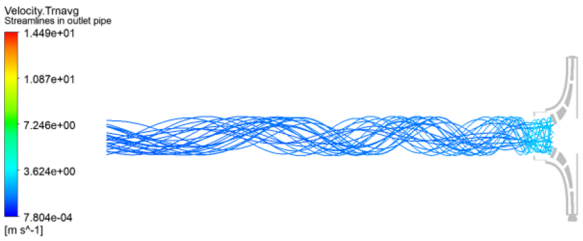

Fig. 20. 2D streamlines in outlet pipe, 1 splitter impeller, n_{11} = 72,12 min^{-1}.

At low n_{11}, the circumferential component of velocity was more dominant relative to the axial component. As n_{11} increased, the axial component increased, and the size of the circumferential component decreased. For a further understanding if this phenomenon is crucial for PaT regime, a more detailed analysis would be necessary, e.g., using vortex identification methods such as Liutex-Rotex or Q-criterion [16].

Hydraulic losses were analysed using entropy production theory for each computational domain. All impeller variants had very similar results. For this reason, results were only presented for the 0splitter and 2splitter variants.

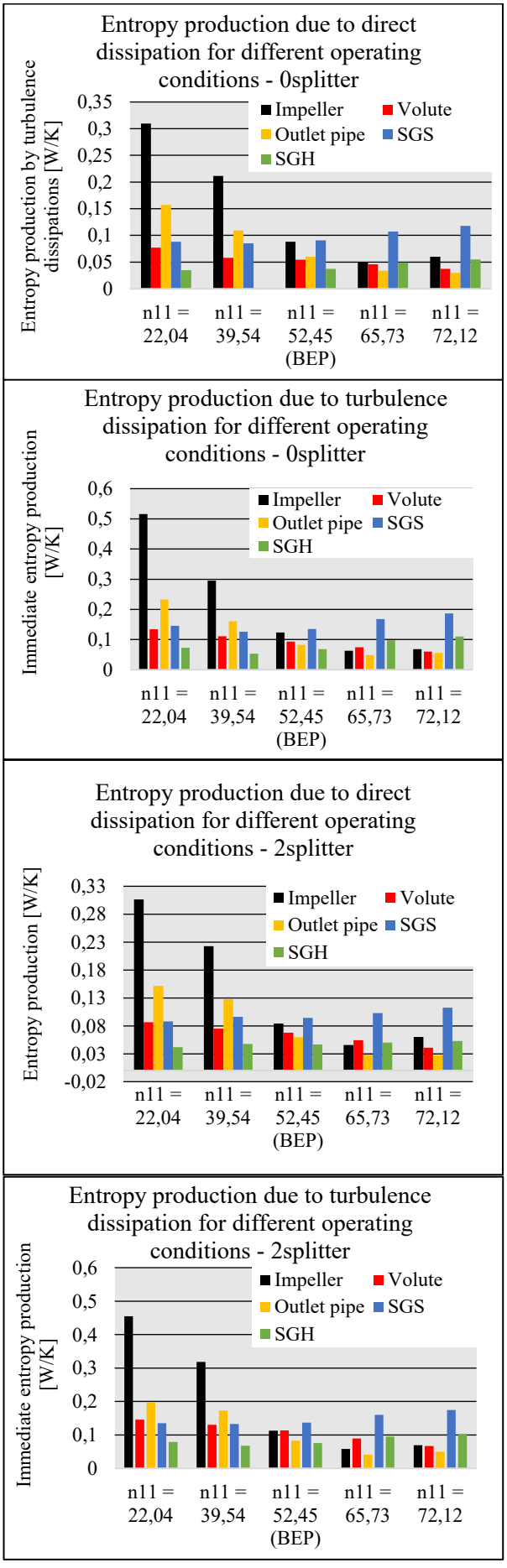

Fig. 21. Quantification of losses in each individual domain for 0splitter and 2splitter.

From the results of the loss analysis, it is clear that in part-load operating conditions, losses inside the impeller dominated. Mainly due to unsteady phenomena such as a local eddy on the suction side of the blade or previously described pumping effect. At part-load operating conditions, there were also significant losses in the outlet pipe, where significant swirling flow appears.

Globally, the losses decreased with increasing unit speed except for the losses in the sidewall gaps, which were in contrast increasing. In this regard, sidewall gap on the shroud side was domain where most significant losses at over-load occurred.

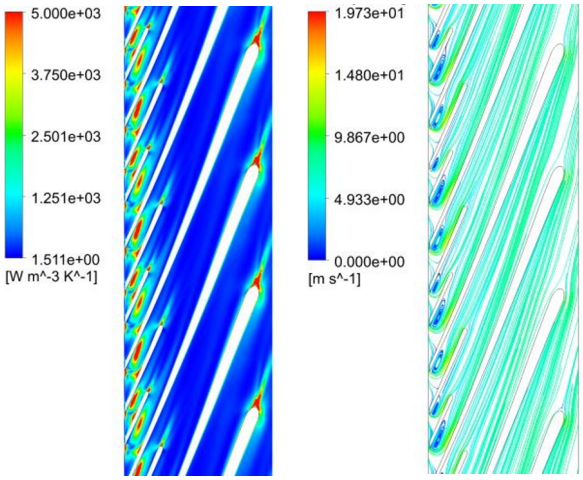

Fig. 22. Density of entropy compared to 2D streamlines in blade to blade view, 2splitter, n_{11} = 22,01 min^{-1}.

The figure 22 shows a comparison of direct entropy production and surface streamlines for the 2splitter variant at the lowest unit speed. It was observed that the locations with increased entropy production correspond to the locations of local eddy on the suction side of the blade. Increased dissipation also occurred in the jet separation region on the pressure side of the blade. The high level of dissipation at the leading and trailing edges of the blades was expected because the blades were exclusively designed for the pump mode and no modifications were made to them.

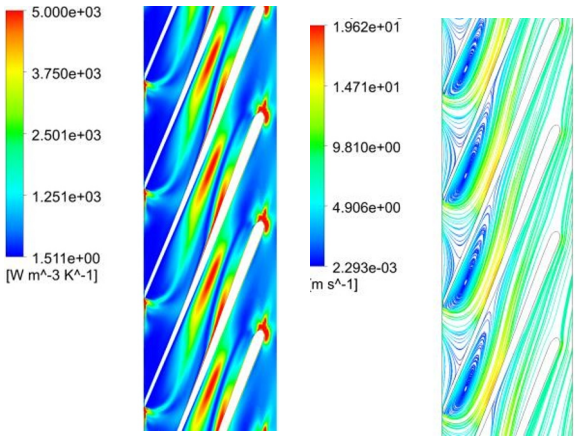

Fig. 23. Direct entropy compared to 2D streamlines in blade-to-blade view, 0splitter, n_{11} = 22,13 min^{-1}.

To investigate the effect of the splitter blades, the above-described quantities were plotted also for the 0splitter variant at the lowest unit speed. The largest area of dissipation which was located on the suction side of the blade has moved downstream. That was the reasonable consequence of the vortex becoming larger in size for the 0splitter variant. Dissipation around trailing and leading edge of blade remained unchanged and shape optimalization for optimal turbine mode performance will be needed.

1splitter layout was chosen for visualization of dissipation areas between different operating conditions of PaT.

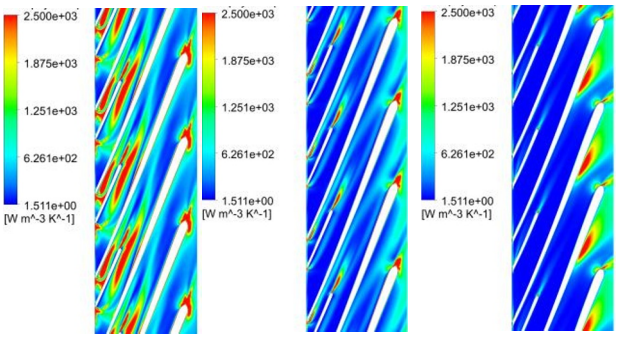

Fig. 24. Direct entropy production in 1splitter impeller for n_{11} = 22,04 min^{-1}, n_{11} = 52,45 min^{-1}, n_{11} = 72,12 min^{-1}.

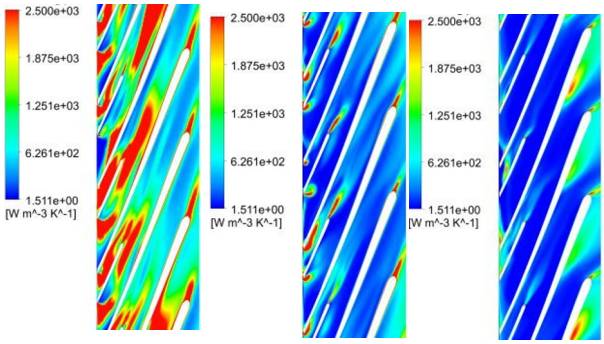

Fig. 25. Instantaneous turbulent entropy production in 1splitter impeller for n_{11} = 22,04 min^{-1}, n_{11} = 52,45 min^{-1}, n_{11} = 72,12 min^{-1}.

From both projected quantities, it was found that the lowest n_{11} operating condition resulted in higher losses, especially in the upper part of the impeller. As n_{11} increased, the losses in this part of the impeller decreased. High losses at the leading and trailing edge of the blade were high in all operating conditions of the PaT. However, at runaway speed n_{11} = 72.12 min^{-1} this loss was shifted against the flow direction. This suggests that the flow deviation was significantly different in this operating condition compared to the other.

Since swirling nature of flow in outlet pipe is well known and negative phenomenon in PaT flow field, more efforts were done to analyse losses in outlet pipe area. For this reason, entropy production near the wall was computed and compared between three impeller layouts.

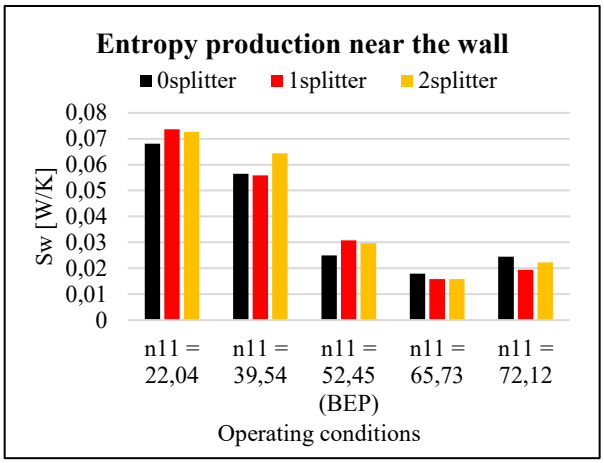

Fig. 26. Entropy production near the wall.

The analysis of entropy production near the outlet pipe wall did not reveal a clear pattern of behaviour between the different impeller variants within the spectrum of unit speeds investigated. This result is expected since the swirl magnitude is mainly driven by the magnitude of impeller rotation.

8 Influence of sidewall gaps

Due to the inclusion of sidewall gaps spaces in the calculation, it was possible to monitor the volumetric efficiency. It was, therefore, possible to quantify the amount of fluid that bypassed the impeller through the space between the shroud and the stator. Thus, a fluid that did not contribute to the torque generation in the impeller.

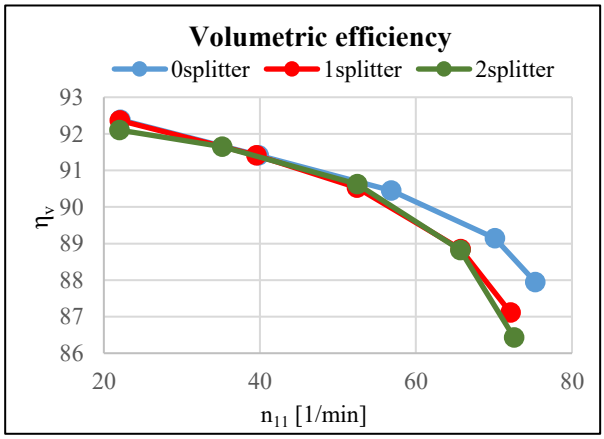

Fig. 27. Volumetric efficiency for each impeller layout.

$$\eta_v = \left(\frac{Q}{Q + Q_{SGS}}\right) \quad (7)$$

The volumetric efficiency η_v was calculated using equation (7), where Q_{SGS} is the flowrate that passes through the space between the impeller shroud disc and the stator. Q is the total flowrate of PaT.

Globally, volumetric efficiency decreased with increasing unit speed and reached low values throughout the range of operating conditions investigated. In the part-load conditions and BEP, the volumetric efficiency was almost the same for all three impeller layouts. In the over-load operating conditions, both variants of the

impellers with splitter blades have the lower volumetric efficiencies. This was caused by the fact that for both splitter blades variants the impeller was more filled due to higher number of blades. In consequence more fluid was bypassing through the sidewall gap around impeller.

Since the volumetric efficiency of the machine was found to be low. Further investigations of flow in the sidewall gaps were necessary. In terms of machine performance, it was important to determine whether the nature of the flow in these spaces contributes to the torque generation or, on the contrary, whether there is dissipation of torque. For this reason, torque on rotating walls in SGS and SGH domains was monitored.

Again, character of behaviour within the investigated operating conditions was the same for all three impeller variants. There was only slight change in absolute number of torque generated or dissipated between them.

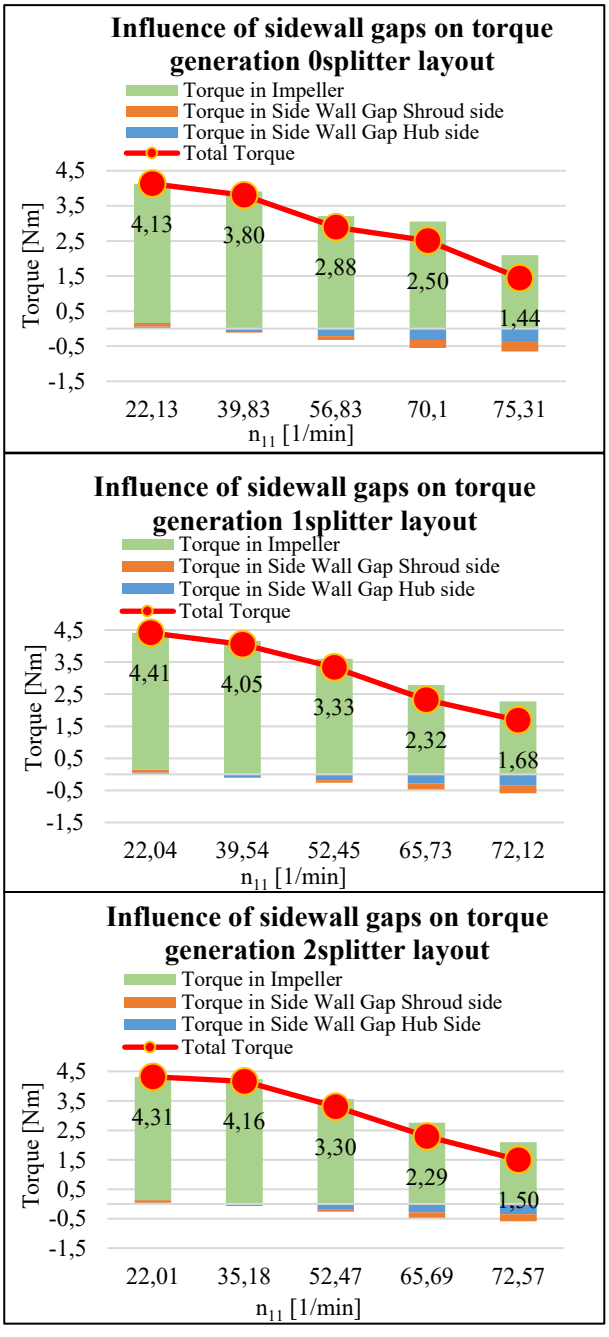

Fig. 28. Sidewall gaps effect on total torque generated by PaT.

It can be seen from the figure that only at the lowest n_{11} the nature of the flow in both sidewall gap spaces was conducive to the generation of the total machine torque. As the unit speed increased, the dissipative character of the flow on the torque generation in these spaces also increased.

The result of this quantitative analysis is that the investigated PaT of low specific speed has low volumetric efficiency. Moreover, the fluid that bypasses the impeller does not contribute to the torque generation in most of the investigated operating conditions and, on the contrary, reduces the total torque of machine. In terms of the computational flow modelling itself, neglecting the domains of sidewall gap spaces would lead to a significant error in machine performance prediction by numerical simulation approach.

9 Hydraulic forces analysis

Hydraulic forces were also monitored during computation. More specifically axial force and radial force were monitored. Time averaged values for different operating conditions for each impeller layout were obtained. For more detailed analysis of dynamic part of forces, Fourier transformation (FFT) was carried out.

The time-averaged values of the axial force show that the magnitude of this force increased with unit speed. There was no significant difference between the 0splitter and 1splitter variants. The 2splitter variant showed lower force magnitudes except for maximum off-design operating conditions. From this it can be concluded that the pressure field in the sidewall gap spaces on which the axial force depends was more uniform. However, the addition of the splitter blades will primarily affect the dynamic pressure field. The static pressure field distribution, hence static part of axial force, should not be significantly affected by the addition of splitter blades.

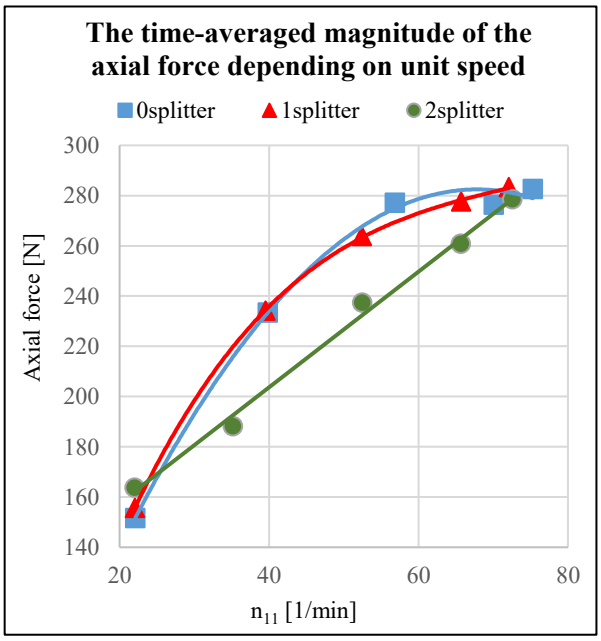

Fig. 29. Time-averaged magnitude of axial force depending on n_{11}.

It was found that the dynamic part of the axial force is low compared to the static component. Force analysis through FFT was done for each of simulated point of characteristic for all three respective impeller cases. Only FFT in BEP for each case is shown. Values of frequencies and amplitudes, including force records plots and amplitude-frequency characteristics for non-optimal operating conditions, might be found in [14].

Table 3. FFT results for 0splitter variant in BEP.

Frequency – Amplitude characteristic 0splitter, BEP	
Relative frequency [-]	Amplitude [N]
4	**12,53**
8	3,89
12	1,94
16	1,08
20	0,56

Table 4. FFT results for 1splitter variant in BEP.

Frequency – Amplitude characteristic 1splitter, BEP	
Relative frequency [-]	Amplitude [N]
4	**5,48**
8	4,24
12	3,23
16	0,51
20	0,55

Table 5. FFT results for 2splitter variant in BEP.

Frequency – Amplitude characteristic 2splitter, BEP	
Relative frequency [-]	Amplitude [N]
4	3,47
8	2,75
12	**3,52**
16	0,28
20	0,64

It was observed that for the variant without splitter blades, blade frequency was dominant. With the addition of splitter blades, the frequency corresponding to the total number of blades, i.e., the splitter-blade frequency was amplified. However, the splitter blade frequency was not always dominant, probably due to the presence of non-stationarities at the interface of the sidewall gap spaces, the impeller and the volute. This was probably due to the influence of the pressure field in the sidewall gaps each time the blade passed around volute tongue.

Furthermore, the radial force was analysed. Time-averaged values showed a decrease in magnitude with increasing the unit speed. Exception was 0splitter variant in low unit speed operating conditions. The values of the radial force magnitude were low with respect to the operating points investigated. Since the values were low, the probability of error in the calculation of the force values was higher.

FFT analysis revealed that the dominant frequency with the highest amplitude value was the rotational frequency for most of the investigated operating conditions. It should be noted that dynamic part of radial force was substantially higher relative to the total value than for the axial force.

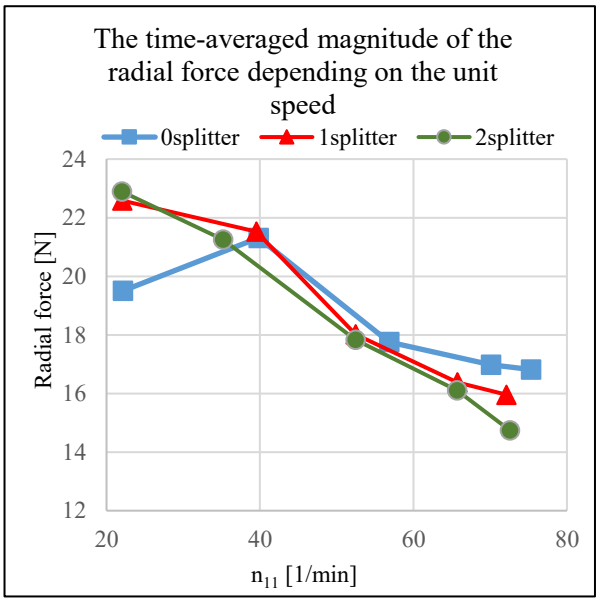

Fig. 30. Time-averaged magnitude of radial force depending on n_{11}.

10 Conclusion

The effect of splitter blades on the turbine mode of a low specific speed pump has been studied. The measured data from the experiment were used to validate the CFD calculation. The numerical approach was used to obtain the PaT characteristics but also to analyse the volumetric efficiency, the effect of sidewall gaps on torque generation and the hydraulic forces. The losses in each domain were evaluated using entropy production theory. For the impeller, the losses were visualized in a blade-to-blade view.

Only a partial influence of the splitter blades on the turbine mode was found. From the experimental data as well as from the CFD calculation, a shift of the optimum (BEP) to lower unit speeds with respect to the 0splitter variant was observed. There was also slight increase of hydraulic efficiency also for impellers with splitter blades.

CFD computed hydraulic efficiency was overestimated compared to the experiment values. The main reason was determined to be the roughness of the physical 3D printed impeller compared to the ideal smooth geometry considered in the numerical model.

Combination of impeller surface roughness and high disk friction losses, which are characteristic for low specific speed machines, probably caused major difference between experiment and CFD values.

The volumetric efficiency of the investigated PaT was found to be low and further decreasing with unit speed. With the exception of the lowest n_{11} operating condition, the flow in both sidewall gaps had a dissipative effect on the total torque generated.

Unsteady phenomena were detected. The most significant are the local eddy in the impeller and the swirling flow in the outlet pipe.

Using the entropy production theory, it was found that at lower n_{11} the losses in the impeller and outlet pipe were dominant. On the other hand, in the over-load operating conditions, the dominant losses were in the sidewall gaps, especially in the shroud side gap. Visualization of losses in the impeller revealed increased losses at the leading and trailing edge of the blades and in locations of local eddies.

Analysis of dissipation was based on articles [15, 16], This approach needs to be further investigated in terms of the correct determination of turbulence-associated dissipation. So that this type of dissipation is not overestimated by combining different approaches.

The time-averaged values of the axial force increased with unit speed. Dynamic component of force was low in comparison with static component. The 0splitter variant had the highest amplitude value at the blade frequency. For the other variants, the total blade frequency, including splitter blades, was always amplified.

The magnitude of radial force decreased with n_{11}. Blade frequency was not dominant as expected. For this reason, further analysis of unsteady phenomena in space between volute, impeller and sidewall gaps will be needed.

Future investigations will include calculations on other meshes with more advanced hybrid turbulence models from the URANS-LES family of models. Efforts to solve the roughness problem, especially on the outside surfaces of the shroud and hub, will be done by either including roughness in the numeric model or by grinding (refining) the physical model. Optimalization and transformation of the geometry of the machine for optimal turbine mode will be carried out to ensure high efficiency not only in BEP but also in part-load and over-load operating conditions, which would increase the possibilities of application of this specific PaT and advantageously, this solution would come close to a classical conventional turbine in terms of power characteristics.

Research was supported by Technology Agency of the Czech Republic under project TK70020001 "Digitalization of water supply infrastructure to optimize the Water-Energy Nexus“ and specific research project FSI FSI-S-20-6235.

References

1. Specific speed. In: *Ksb.com: KSB Circular Pump Lexicon - from A to Z* [online]. KSB [cit. 2022-11-10]. Available from: [CrossRef], [CrossRef2].
2. R Klas, F. Pochylý, P. Rudolf *IOP Conf. Ser.: Earth Environ. Sci.* **22** 012010 (2014)
3. L. Chabannes, D. Štefan, P. Rudolf, Energies, Effect of Splitter Blades on Performances of a Very Low Specific Speed Pump, **14** (2021)
4. C. Santolaria, J. Oro, K. Díaz, Int. J. Numer. Methods Fluids, Numerical modelling and flow analysis of a centrifugal pump running as a turbine: Unsteady flow structures and its effects on the global performance, **65**, 542 - 562 (2011)
5. A. S. Aidhen, S. Malik, C. D. Kishanrao, Int. J. of Engineering and Advan. Technol. (IJEAT), Turbine Mode Performance Evaluation of Centrifugal Pump, **9**, 2249-8958 (2019)
6. Md. Rakibuzzaman, K-Y. Jung, S-H. Suh, E3S Web of Conferences, A study on the use of existing pump as turbine, **128**, 06004 (2019)
7. W-G. Li, Appl. Math. Model., Effects of viscosity on turbine mode performance and flow of a low specific speed centrifugal pump, **40**, 904-926 (2016)
8. Y. Sun-Sheng et al, Int. J. Rotating Mach., Numerical Research on Effects of Splitter Blades to the Influence of Pump as Turbine, **2012** (2012)
9. L. Chabannes, Dissertation thesis, VUT Brno FSI, Design of Very Low Specific Speed Pump (2021)
10. V. Sanjay et al., Renewable Sustainable Energy Rev., Investigations on pump running in turbine mode: A review of the state-of-the-art, **30**, 841-868 (2014)
11. V.A. Patel, S.V. Jain, K.H. Motwani, R.N. Patel, Procedia Eng., Numerical Optimization of Guide Vanes and Reducer in Pump Running in Turbine Mode, **51**, 797-802 (2013)
12. M. Stefanizzi et al, AIP Conf. Proc., Pump as turbine for throttling energy recovery in Water Distribution Networks, **2191**, 020142 (2019)
13. A. Carravetta et al, Energies, PAT Design Strategy for Energy Recovery in Water Distribution Networks by Electrical Regulation, **6**, 411-424 (2013)
14. J. Bezdíček, Diploma thesis, VUT Brno FSI, Low specific speed pump working in turbine mode (2022)
15. P. Huang, D. Appiah, K. Chen, F. Zhang, P. Cao, Q. Hong, AIP Advances **11**, 045208 (2021)
16. C. T. Tran, D. C. Pham, Teh. Vjesn., Application of Liutex and Entropy Production to Analyze the influence of vortex Rope in the Francis-99 Turbine Draft Tube, **29**, 1177-1183 (2022)

17. K. Juckelandt, F-H. Wurm, In Proceedings of the ASME Turbo Expo 2015: Turbine Technical Conference and Exposition, Applicability of Wall-Function Approach in Simulations of Turbomachines, **Volume 2B: Turbomachinery**, GT2015-42014, V02BT39A001; 10 pages (2015)
18. L. Chabannes, D. Stefan, P. Rudolf, IOP Conference Series: Earth and Envi. Sci., Volute throat area and wall modelling influence on the numerical performances of a very low specific speed pump, **774**, 012007 (2021)
19. Y Wang and W J Wang 2012 *IOP Conf. Ser.: Earth Environ. Sci.* **15**, 062013 (2012)